Understanding the photoelectrochemical properties of a reduced graphene oxide-WO_3 heterojunction photoanode for efficient solar-light-driven overall water splitting

Jingdong Lin,[a,b] Peng Hu,[c] Yan Zhang,[a] Meiting Fan,[b] Ziming He,[a] Chee Keong Ngaw,[a]
Joachim Say Chye Loo,*[c] Daiwei Liao,[b] and Timothy Thatt Yang Tan*[a]

[a] *Solar Fuel Lab, School of Chemical and Biomedical Engineering, Nanyang Technological University, Singapore 637459. E-mail: tytan@ntu.edu.sg*

[b] *Department of Chemistry, College of Chemistry and Chemical Engineering, Xiamen University, Xiamen, 361005, China.*

c Solar Fuel Lab, School of Materials Science and Engineering, Nanyang Technological University, Singapore, 639798. E-mail: Joachimloo@ntu.edu.sg

* CORRESPONDING AUTHOR, E-mail: tytan@ntu.edu.sg, Joachimloo@ntu.edu.sg

1. Experiment details

Natural graphite powder (325 meshes) was commercially obtained from Alfa-Aesar. 37% hydrochloric acid (HCl), 98% sulfuric acid (H_2SO_4), 25% ammonia solution, 30% hydrogen peroxide (H_2O_2), potassium manganese oxide ($KMnO_4$), sodium nitrate ($NaNO_3$), potassium persulfate ($K_2S_2O_8$) and phosphorus pentoxide (P_2O_5), poly vinyl pyrrolidone (PVP) (K value = 29~32) and ammonium metatungstate hydrate (AMT), were supplied by Sigma. All reactants were used as received. Argon (Ar) and nitrogen (N_2) were supplied by National Oxygen Pte Ltd Singapore.

1.1 Preparation of Graphene Oxide (GO). GO was produced using a modified Hummers method.[1-3] In detail, $K_2S_2O_8$ (10.0 g) and P_2O_5 (10.0 g) were dissolved in 98% H_2SO_4 (50.0 mL) at 80 °C. Graphite powder (12.0 g) was added to the above acidic solution, and the resulting mixture was stirred at 80 °C for 4.5 hrs. After cooling to room temperature, the solution was diluted with 2.0 L de-ionized (DI) water and stood overnight. The pretreated graphite was obtained by centrifugation and washed three times with DI water. The product obtained was dried in air at 100 °C for 12 hrs. This pretreated graphite powder (2.0 g) was put into 98% H_2SO_4 (46.0 mL) at ice bath. $KMnO_4$ (6.0 g) and $NaNO_3$ (2.0 g) were added gradually under stirring, and the solution was kept at ice bath for 30 min. The mixture was then stirred at 35 °C for 15 hrs and then DI water (96.0 mL) was added at ice bath temperature. The reaction was then terminated by adding DI water (300 mL) and 30% H_2O_2 solution (5.0 mL). The mixture was centrifugation and subjected to suspension in 3% HCl solution and separated by centrifugation. In order to completely remove metal ions and acids, the GO was washed with DI water and separated with centrifugation until the pH value of the supernatant reached 6. The GO product was suspended in DI water to give a viscous, brown dispersion.

1.2 Synthesis of WO_3/RGO composites. WO_3/RGO composites were prepared by thermal treatment method, using GO as a precursor of RGO, AMT as a precursor of WO_3, and PVP as an intermediate to combine tungsten with GO.[4] Briefly, 2.5 g PVP was dissolved in 12.0 mL DI water to form solution A. 10.0 g AMT was dissolved in 6.0 mL DI water (pH = 4.0) to form solution B. 9.0 mL 11 mg/mL GO solution was ultrasonicated for 2 hrs labeled as solution C. Solution B and C were added to solution A under stirring at room temperature simultaneously. The mixture was ultrasonicated for 30 min and then stirred for 4 hrs to obtain WO_3/GO precursor solution. Samples without GO were also fabricated using a similar procedure for comparison. The WO_3 and WO_3/RGO electrodes were prepared by dip-coating technology using above precursor solutions on fluorine-doped tin oxide (FTO) glass (Nippon Sheet Glass, 10*25 mm, 15Ω/square) and calcined at 450 °C for 5 hrs in air. WO_3 and WO_3/RGO powders were also obtained by calcining precursors at 450 °C for 5 hrs in air for ultraviolet-visible diffuse reflection spectroscopy (UV-vis/DRS), transmission electron microscopy (TEM) and Fourier transform-infrared (FTIR) characterizations.

1.3 Characterization and measurements

The morphology and thickness of the obtained GO were evaluated by atomic force microscopy (AFM, Asylum Research, MFP 3D). TEM and energy-dispersive X-ray measurements (EDX) were carried out on a JEOL 2100 microscope at 200 kV. TEM specimens were prepared by dispersing powder in ethanol and picked up with holey carbon supporting films on copper grids. Thermal gravimetric analysis (TGA) was conducted on a SDT Q600 instrument with a heating rate of 10 °C/ min under air flow. A Nicolet 6700 FT-IR spectrometer equipped with MCT/A detector was used in this study. 32 scans were recorded in the absorbance mode at a 4 cm^{-1} resolution. For *in-situ* FTIR characterization of GO, a 13-mm diameter self-supporting disk of GO-KBr (*w/w*=1/100) was treated under air flow in IR cell at different temperatures and the FTIR spectra were recorded. The surface morphologies and cross-sections of electrodes were observed using Field emission scanning electron microscopy (FESEM, JEOL JSM-6700F). Raman spectra were obtained using a Renishaw inVia Raman microscope with excitation wavelength at 514.5 nm. X-ray powder diffraction (XRD) patterns were recorded using Panalytical X`pert Pro Super X-ray diffractometer with Cu Kα radiation ($\lambda = 0.15418$ nm). The accelerating voltage of 40 kV and emission current of 30 mA were used. The 2θ angular regions between 10° and 80° were recorded at a scan rate of 0.0167 ° for 10 s. The specific surface area was measured with a pore and surface analyzer (Quantachrome Adsorb-6B) and calculated using the Brunauer-Emmett-Teller (BET) equation. UV-vis/DRS were recorded using a Varian Cary 5000 UV-vis spectrophotometer. $BaSO_4$ was used as a reference. The band gap (E_g) is obtained based on diffuse reflectance measurements using Kulbeka–Munk function and Tauc theory.[5] The following expression proposed by Tauc et al. is used.

$$[F(R)\,h\nu]^{1/n} = A(h\nu - E_g) \ldots\ldots\ (1)$$

Where: h: Planck's constant, ν: frequency of vibration, $F(R)=(1-R)^2/2R$, where R is the percentage reflectance, E_g: band gap, A: proportional constant, the value of the exponent n of WO_3 is 2. The band gap energies are calculated from their diffuse reflectance spectra by plotting the $[F(R)\,h\nu]^{1/2}$ versus hν (eV). The line tangent to the plotted curve inflection point is extrapolated to $[F(R)\ h\nu]^{1/2} = 0$ to get the band gap energy.

For investigating the photoelectrochemical properties of the prepared electrodes, a common three-electrode system was used. All the photoelectrochemical measurements were carried out in common three-electrode cell with quartz window using 0.5 M H_2SO_4 aqueous solution as electrolyte. The electrolyte was purged by Ar or N_2 for 30 min to avoid the effect of oxygen prior to experiments. The counter electrode was a platinum grid and Ag/AgCl was used as reference electrode. The prepared electrodes were used as working electrodes. The working surface area was 0.2 cm^2. The light source was simulated sunlight from a 150 W xenon solar simulator (67005, Newport Corp.) through an Air Mass filter (AM1.5 Global, 81094) with a measured intensity equivalent to standard AM1.5 sunlight (100 mW/cm^2) at the sample face.

The photocurrent-time plots and linear sweep voltammetry (LSV) characteristics of electrodes were measured by an electrochemical analyzer (CHI 852C) under chopped solar simulator illumination. Applied bias photon-to-current efficiency (ABPE) was calculated by: [6]

$$\text{ABPE}\% = (|J\ (\text{mA/cm}^2)| \times (1.23\text{-}V_b)\ (\text{V}))/P_{total}\ (\text{mW/cm}^2) \times 100\% \ldots.\ (2)$$

where J is the photocurrent density obtained under an applied bias V_b. P_{total} is the total integrated power input density (100 mW/ cm^2).

Electrochemical impedance spectroscopy (EIS) was performed using Autolab PGSTAT 302N system equipped with the FRA2 Faraday impedance module with frequency range from 0.01 Hz to 100 kHz at 10 mV of amplitude potential under illumination. The semiconducting properties of the films were analyzed and the related parameters were calculated by the Mott–Schottky equation.

$$1/C^2 = (2/q*\varepsilon*\varepsilon_0*N_D)[(U-U_{fb})-kT/q] \ldots\ldots\ldots..\ (3)$$

Where, C is the electrode capacitance, q is the electron charge, ε is the dielectric constant of WO_3, ε_0 the permittivity of vacuum, U is the applied potential, U_{fb} is flat band potential, *k* is the Boltzmann constant, T is the temperature, N_D is the concentration of carrier.

Incident photon to electron conversion efficiency (IPCE) characteristics were measured with a 500 W xenon light source (Newport, 66983) coupled with a monochromator (Newport, 74125) at a potential of 1.0 V vs Ag/AgCl. A Si photodiode (Bentham, DH-Si) with known IPCE was used to calculate the IPCE of the photoanodes. A source meter (Keithley Instruments Inc., Model: 2400) was used to measure the photocurrent of Si diode. The electrochemical analyzer (CHI 852C) mentioned above was used to measure the photocurrent of samples. The equation for IPCE calculation was as following:

$$\mathrm{IPCE}(\lambda) = 100*1240*j(\lambda)/\lambda/I(\lambda) \quad \ldots\ldots\ldots\ldots(4)$$

Where λ is the wavelength of light in units of nm, j(λ) is the photocurrent density in $\mathrm{mA/cm^2}$ under illumination at λ, and I(λ) is the incident-light intensity in $\mathrm{mW/cm^2}$ at λ. By convolving the IPCE curve with the photon flux, I(λ), derived from the AM1.5 spectrum, an estimate of the photocurrent under AM1.5 illumination can be calculated by:[7]

$$j_{\mathrm{calculated}} = \int_0 IPCE(\lambda) * I(\lambda) * \frac{\lambda(nm)}{1240} * d\lambda \quad \ldots\ldots\ldots(5)$$

The electrochemical analyzer (CHI 852C) mentioned above was used for photocatalytic overall water splitting. During overall water splitting, hydrogen and oxygen were measured by a gas chromatograph (GC, HP6890A) with a thermal conductivity detector (TCD) and molecular sieve 5Å column using Ar as the carrier gas. For this purpose, the PEC cell was used with closed parts and the amount of H_2 and O_2 produced in the head space of the cell were measured by applying a constant bias potential of 1 V vs Ag/AgCl under solar simulator illumination.

As shown in Scheme 1, the Schottky barrier height (SBH) can be calculated by:

$$\varphi_M = \varphi_0 - \Delta E_F \quad \ldots\ldots\ldots\ldots(6)$$

Where, φ_M is SBH, φ_0 is the difference between interface states and CB of WO_3, ΔE_F is difference of Fermi level of interface states.

2. Supporting figures and discussion.

The oxygen functional groups on GO sheets are not only in favor of the formation stable GO water solution, but also provide abundant sites for precursors loading which is beneficial to the formation of uniform semiconductor/RGO composites.[8] Therefore, GO was used as the raw material to prepare WO_3/RGO. Fig. S1 shows the TEM, AFM images and height profile of GO along the line shown in AFM image of GO. Thin GO sheets with wrinkles are observed. The AFM image of GO shown in Fig. S1b indicates most GO contains single layer with size around 0.5 ~ 4 μm. In addition, the thickness of GO sheets is ~ 0.92 nm, larger than that of pristine graphite (0.34 nm), indicating a full exfoliation of graphite oxide. Figure S1 indicates that GO contains single layer with size around 0.5 ~ 4 μm was successfully prepared by modified Hummers method.[1]

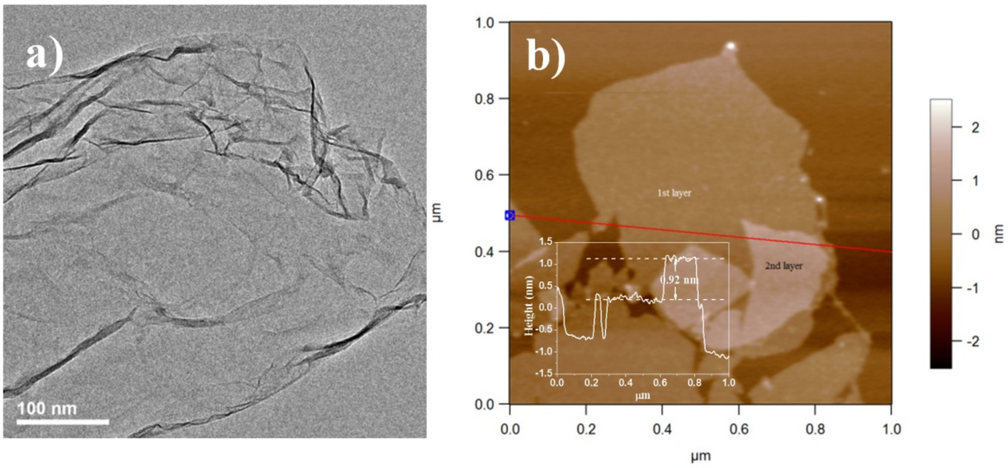

Fig. S1 (a) TEM image of GO sheets; (b) AFM image of GO sheets and height profile of GO along

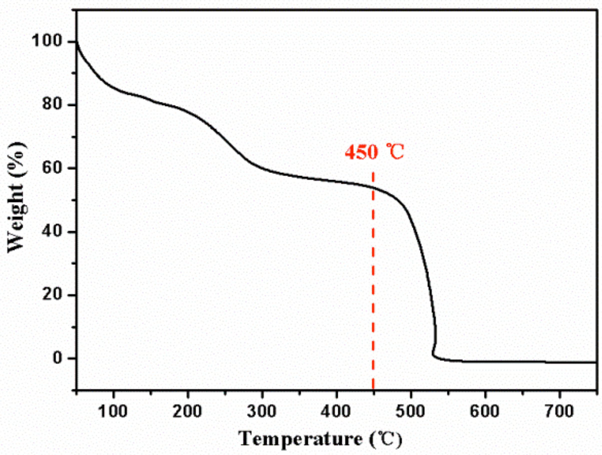

Fig. S2 TGA curve of GO in air flow.

Calcination is a common way to achieve WO_3 crystal. In the meantime, thermal treatment is an effective method for reduction of GO.[9] Therefore, the reduction of GO and crystallization of WO_3 to fabricate WO_3/RGO composites were simultaneously achieved through calcination. In order to obtain the relevant information of GO transformation by thermal treatment, TGA and *in-situ* FTIR experiments were carried out. As shown in Fig. S2, GO shows a significant weight loss at ~250 °C and good thermal stability until 450 °C. *In-situ* FTIR spectra of GO obtained at different temperatures are shown in Fig. S3. The broad band at ~ 3200 cm^{-1}, which is ascribed to absorbed water and hydroxyl,[10] significantly decreases with increasing temperature and almost disappears at 450 °C. The bands at 1730, 1620, 1400 and 1100 cm^{-1}, which are assigned to C=O stretching vibrations in carboxylic acid, deformation vibration of hydroxyl, O-H deformation vibration and C-O stretching vibration, respectively,[11] show the similar trend of the band at ~ 3200 cm^{-1}. The FTIR results show that RGO has significantly less oxygen functional groups than GO after thermal treatment at 450 °C, which is consistent with the TGA analysis, demonstrating the successful thermal reduction of GO to RGO by thermal treatment at 450 °C.

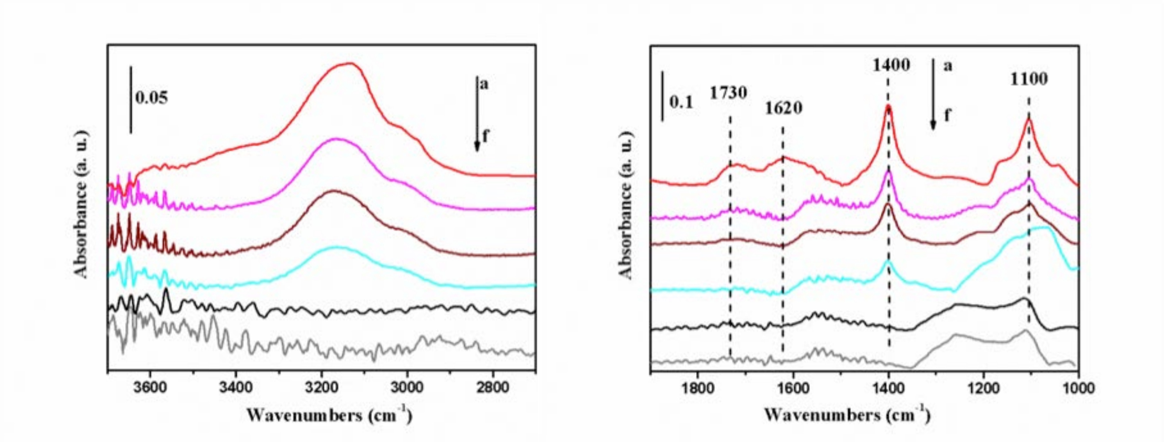

Fig. S3 *in-situ* FTIR spectra of GO obtained at different temperatures.
(a: 50 °C; b: 150 °C; c: 250 °C; d: 350 °C; e: 450 °C; f: 500 °C)

FTIR spectra of WO_3 and WO_3/RGO dried at 120 °C and 450 °C were shown in Fig. S4. The bands attributed to PVP were disappeared completely at 450 °C. The FTIR results indicate that PVP can be removed from WO_3 or WO_3/RGO precursors by calcination at 450 °C under air. Similar results were reported in ZnO/RGO composites prepared by the similar method.[6] Therefore WO_3/RGO composites are fabricated by calcination at 450 ^{0}C.

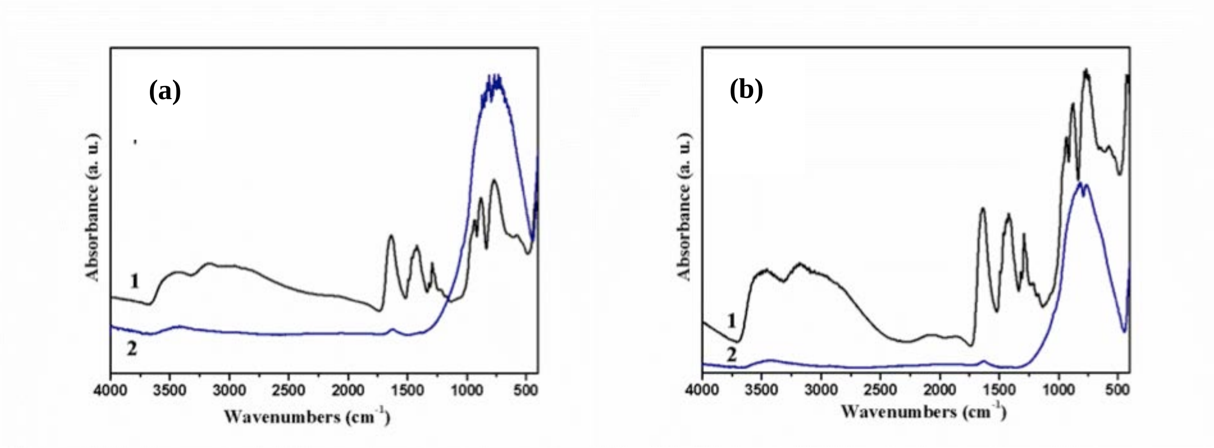

Fig. S4 FTIR spectra of (a) WO_3/RGO and (b) WO_3 calcined at different temperatures.
(1: 120 °C overnight; 2: 450 °C for 5 hrs)

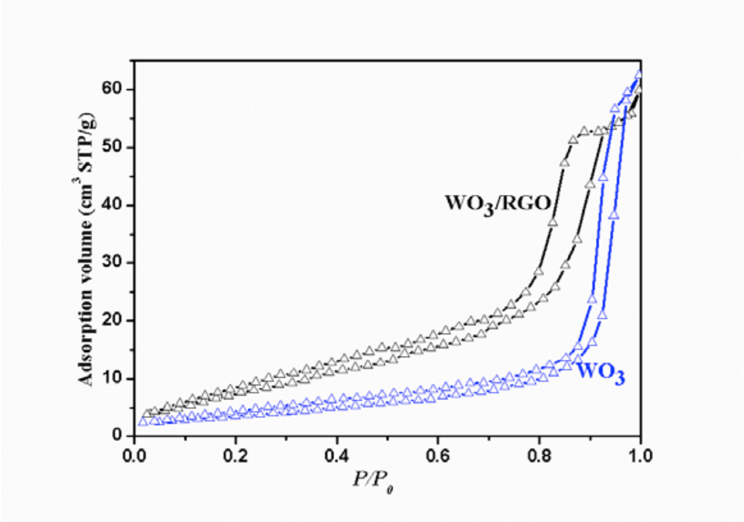

Fig. S5 Nitrogen adsorption-desorption isotherms of WO_3 and WO_3/RGO.

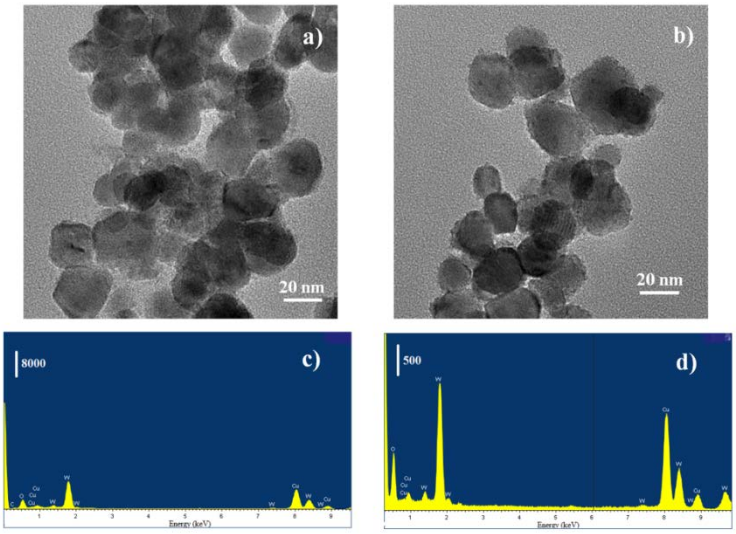

Fig. S6 TEM images of (a) WO_3/RGO and (b) WO_3; EDX images of (c) WO_3/RGO and (d) WO_3.

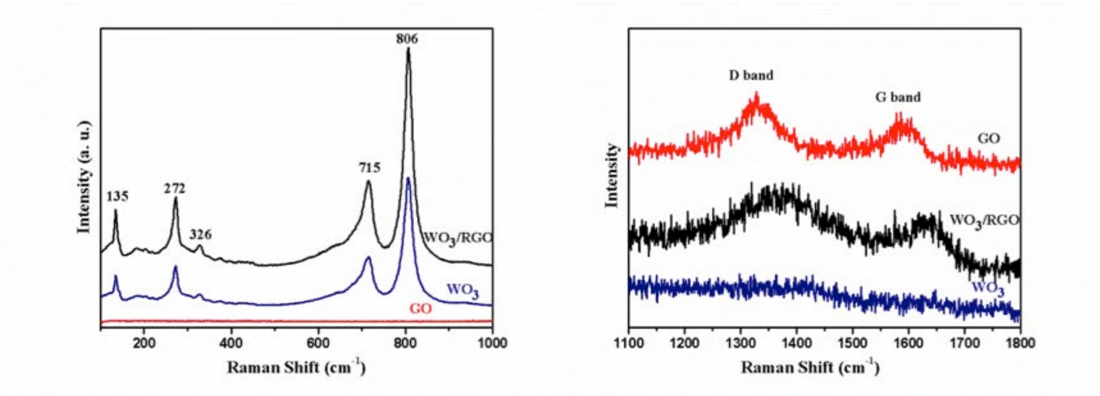

Fig. S7 Raman spectra of WO_3, WO_3/RGO and GO.

The Raman spectra of WO_3, WO_3/RGO and GO over the ranges of 100-1000 cm^{-1} and 1100-1800 cm^{-1} are shown in Fig. S7. The two main intense peaks at 806 and 715 cm^{-1}, and the shoulder at ~ 680 cm^{-1}, are typical Raman peaks of crystalline WO_3, which correspond to W–O stretching (υ), W–O bending (δ) and O–W–O deformation (γ) modes, respectively.[12] Two peaks at 326 and 272 cm^{-1} are assigned to the bending δ (O–W–O) vibrations. The peak at ~ 135 cm^{-1} is attributed to the lattice vibrations of WO_3.[12-13] As for GO, two peaks at ~ 1340 and 1590 cm^{-1} are typical Raman peaks of GO, which correspond to the D-band and G-band, respectively.[14] There is no Raman peak observable over the range of 1100-1800 cm^{-1} for WO_3 electrode. The G-band up-shift from 1590 to 1610 cm^{-1} are observed for WO_3/GRO compared with GO. The bands up-shift are generally evidences of chemical doping of carbon materials, suggesting charge transfer between the RGO and WO_3 in the WO_3/RGO composite.[15] The Raman results indicate that RGO firmly interacts with WO_3 and WO_3/RGO electrode is successfully fabricated.

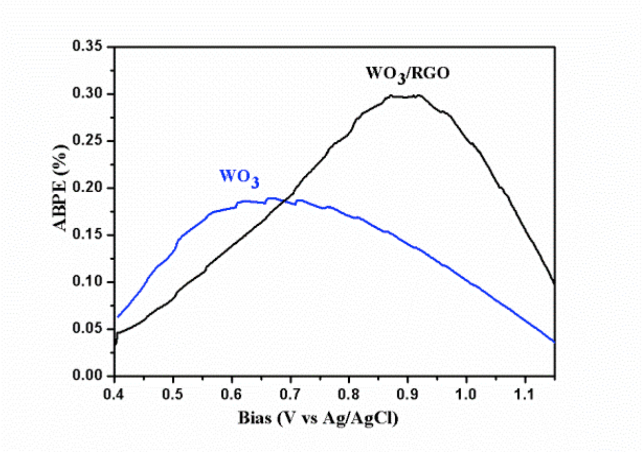

Fig. S8 ABPE of WO_3 and WO_3/RGO electrodes.

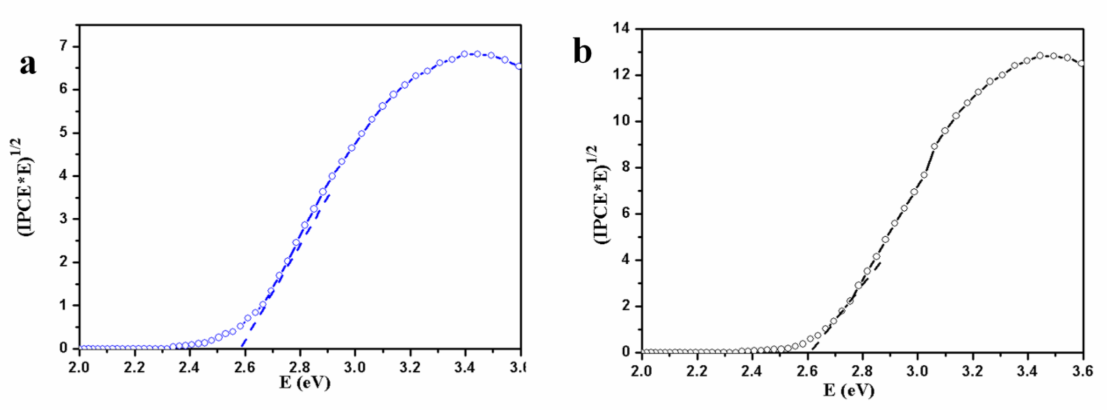

Fig. S9 Tauc plots of (a) WO_3 and (b) WO_3/RGO derived from the IPCE shown in Fig. 3d.

REFERENCES

1. W. S. Hummers and R. E. Offeman, *J. Am. Chem. Soc.*, 1958, **80**, 1339.
2. J. Geng and H. Jung, *J. Phys. Chem. C*, 2010, **114**, 8227.
3. N. I. Kovtyukhova, P. J. Ollivier, B. R. Martin, T. E. Mallouk, S. A. Chizhik, E. V. Buzaneva and A. D. Gorchinskiy, *Chem. Mater.*, 1999, **11**, 771.
4. Y. Yang, L. L. Ren, C. Zhang, S. Huang and T. X. Liu, *ACS Appl. Mater. Interfaces*, 2011, **3**, 2779.
5. J. Tauc, R. Grigorovici and A. Vancu, *Phys. Stat. Sol.*, 1966, **15**, 627.
6. Z.B. Chen, T. F. Jaramillo, T. G. Deutsch, A. Kleiman-Shwarsctein, A. J. Forman, N. Gaillard, R. Garland, K. Takanabe, C. Heske, M. Sunkara, E. W. McFarland, K. Domen, E. L. Miller, J. A. Turner and H. N. Dinh, *J. Mater. Res.*, 2010, **25**, 3.
7. B. Yang, Y. J. Zhang, E. Drabarek, P. R. F. Barnes and V. Luca, *Chem. Mater.*, 2007, **19**, 5664.
8. J. Kim, L. J. Cote, F. Kim, W. Yuan, K. R. Shull and J. X. Huang, *J. Am. Chem. Soc.*, 2010, **132**, 8180.
9. G. Eda, C. Mattevi, H. Yamaguchi, H. Kim and M. Chhowalla, *J. Phys. Chem. C*, 2009, **113**, 15768.
10. H. L. Guo, X. F. Wang, Q. Y. Qian, F. B. Wang and X. H. Xia, *ACS Nano*, 2009, **3**, 2653.
11. C. Hontoria-Lucas, A. J. López-Peinado, J. D. López-González, M. J. Rojas-Cervantes and R. M. Martín-Aranda, *Carbon*, 1995, **33**, 1585.
12. A. Nonaka and A. Takase, *J. Mater. Sci. Lett.*, 1993, **12**, 274.
13. O. Yayapao, T. Thongtem, A. Phuruangrat and S. Thongtem, *J. Alloys Compd.*, 2011, **509**, 2294.
14. S. Stankovich, D. A. Dikin, R. D. Piner, K. A. Kohlhaas, A. Kleinhammes, Y. Y. Jia, Y. Wu, S. T. Nguyen and R. S. Ruoff, *Carbon*, 2007, **45**, 1558.
15. J. J. Guo, Y. Li, S. M. Zhu, Z. X. Chen, Q. L. Liu, D. Zhang, W. J. Moon and D. M. Song, *RSC Advances*, 2012, **2**, 1356.